Development and test of an IR camera for astronomical observation at the Palomar 200-inch observatory using the NICMOS II array

Carl F. Bruce, Charles A. Beichman, Dale Van Buren, Thomas Nicholas Gautier, Carlos R. Jorquera, et al.

Carl F. Bruce, Charles A. Beichman, Dale Van Buren, Thomas Nicholas Gautier, Carlos R. Jorquera, Kirk L. Seaman, "Development and test of an IR camera for astronomical observation at the Palomar 200-inch observatory using the NICMOS II array," Proc. SPIE 1762, Infrared Technology XVIII, (5 January 1993); doi: 10.1117/12.138986

SPIE.

Event: San Diego '92, 1992, San Diego, CA, United States

Development and test of an IR camera for astronomical observation at the Palomar 200-in. Observatory using the NICMOS II Array

Carl Bruce, Charles Beichman, D. Van Buren, Nick Gautier,
Carlos Jorquera, and Kirk Seaman

Jet Propulsion Laboratory, California Institute of Technology
Pasadena, California 91109

ABSTRACT

A NICMOS II Array has been integrated into the California Institute of Technology's Palomar Observatory Camera. Using commercially available electronics and custom software, the camera has been fully tested and characterized. The PC-based system has been successfully used for astronomical observations at the 5-m Hale Telescope at the Palomar Observatory. Performance and calibration data are given.

1. INTRODUCTION

A near-infrared (0.80- to 2.6-μm) imaging system has been developed and integrated using almost all commercially available components. The camera system has been tested and operated in a science mode at the Hale Telescope at the California Institute of Technology's Palomar Observatory Facility. This joint effort between engineers and scientists at the Jet Propulsion Laboratory and the California Institute of Technology has given these institutions a science-grade observing capability in the near infrared.

2. SYSTEM DESCRIPTION

The Palomar camera system consists of six discrete subsystems: the focal plane, the electrical interface, the drive and data acquisition electronics, the dewar, the dewar optics and the software. Each subsystem will be described and the relevant performance and calibration data will be given. Test data on the focal plane performance will be reviewed in detail and the results of some astronomical observations will be presented.

2.1. The focal plane

The short-wavelength infrared focal plane used in this system is a 128- × 128-pixel HgCdTe photovoltaic detector array, commonly referred to as the NICMOS II Array. Work is currently under way to upgrade the system to accommodate the 256- × 256-pixel NICMOS III Array. These arrays are produced by Rockwell International under a NASA-funded contract through the University of Arizona.[1] The NICMOS III Array is a commercial product available from Rockwell International.

The infrared array is a matrix of 128 × 128 photodiodes formed by ion implantation into a layer of HgCdTe grown on a sapphire substrate. The HgCdTe layer is grown using liquid phase epitaxy techniques. The band gap of the photovoltaic detectors is tuned to a 2.6-μm cutoff wavelength by choosing the appropriate concentrations of Cd and Hg.[2] The 128 × 128 HgCdTe photodiode array is mated electrically, through indium column bump bonds, to a silicon multiplexer. The silicon multiplexer is a matrix of 128- × 128-PMOS unit cells. These unit cells operate on a back-bias principle with a switched source follower multiplexer.

A circuit diagram of the readout is presented in Fig. 1. The focal plane array (FPA) is operated by resetting the integration node (A) to about -0.5 V relative to the photodiodes' cathode, through the action of the reset switch (B). Photons entering the optically active region with an energy greater than the HdCdTe band gap create electron hole pairs, which are integrated onto the capacitance of node (A). This capacitance is the sum of the MOSFET gate reverse-bias capacitance, the diode reverse-bias capacitance, and the stray capacitances due to the layout geometry. After an integration time defined by the user, the voltage now present at node (A) is passed by the source follower created by MOSFETs (C) and (D) to the gate of the output MOSFET (E), where it may be read out by a variety of circuit schemes.

 0-8194-0935-9/92/$4.00

Each pixel of the array is sequentially read out in this manner via the action of CMOS shift registers, which supply the column and row select clock pulses. Various multiplexing schemes are configurable with slight timing variations. The nominal timing configuration sequentially resets each pixel, integrates for a preselected time, and then sequentially reads each pixel. In this way, the integration time seen by each pixel is of identical length but shifted in time by one pixel clock time as shown in Fig. 2. This has the effect of defining the minimum integration time possible for the array as the product of the number of pixels and the pixel rate. The nominal data rate is 125 kHz, giving a minimum integration time of 0.13 s for the system.

2.2 The electrical interface

The electrical interface to the NICMOS II array consists of 4 clocks and 17 biases with 2 test points. Fortunately, the number of required unique biases is 6 because 11 of the biases may be tied directly to Vdd or ground. The electrical interface from the focal plane to the 32-pin Bendix connector, which is located on the dewar's outer wall, is summarized in Table 1.

On all clock lines, constantan wire is used to reduce the heat load to the dewar, even though such loads are not expected to be more than a milliwatt or two. Additionally, 100-Ω resistors are connected in series with the clock inputs, which are expected to draw zero current. This helps to reduce ringing and coupling at the clock inputs. Low-impedance copper wire is used on Vdd and Vss to reduce voltage drops on the wire induced by current fluctuations to the array before and after integrations. Stainless-steel micro coaxial wire is used to shield the most sensitive multiplexer lines. These lines are the source output, both the anode and the cathode of the photodiode and the PGate, which is the switched source follower load.

The shields of these coaxial lines are tied to ground at the drive electronics box and floated at the multiplexer inputs in an effort to avoid ground loops on the shields. Impedances for each line are given in Table 1. To shunt high-frequency noise on the dc supplies, 0.10- and 4.7-μF capacitors are used as bypass capacitors. PGate is additionally filtered with an RC network to limit bias drifts to a time constant of 1.7 s.

All components are mounted on a circuit card located in the dewar (Fig. 3). The Teledyne D205-025 board-to-flexible-cable connectors are used for mating with the NICMOS II chip carrier. The chip carrier is a 32-lead, quad in-line package produced by GE ceramics (part number ST 88036L1-D1). The circuit card has a ground plane with a single point ground at Vss. Special care was taken to ensure that the dewar remains electrically isolated from the focal plane. This is because the dewar is mated to the Hale Telescope and thus held at the potential of the telescope. This grounding strategy provides the FPA with an environment well shielded from the effects of EMI.

2.3 The drive and data-acquisition electronics

The drive and data acquisition electronics, Model 300, are purchased from RAPAX Systems and Engineering of Honolulu, Hawaii. The system is PC based with two expansion boards for the generation of array and camera control signals and for the buffering of array data. The two buffers can handle arrays of up to 256 × 256 pixels. The bulk of the hardware (i.e., four preamplifiers, a 16-bit analog-to-digital converter, digital timing circuitry, and a high-speed data transmitter) is enclosed in a 24- × 12-in. steel box divided into four separate compartments. The box is fixed directly to the dewar on an insulating, plexiglass mounting plate. A high-speed data receiver located at the PC completes the data link for the transfer of image data from the camera electronics to the PC.

The system is compatible with both the NICMOS II and III Arrays with their 128^2- and 256^2-pixel formats, respectively. To accommodate the four outputs of the NICMOS III Array, the camera electronics are configured with four input preamplifiers, each with a differential input stage and current source for the NICMOS output PFETS. Offset and moderate gain are provided by the preamplifiers, which use ultralow-drift operational amplifiers. For operation with the NICMOS III device, the four preamplifiers are sequentially multiplexed into a single 16-bit analog-to-digital converter with a minimum acquisition time of 2 μs. With the NICMOS II device, only one preamplifier is used and the multiplexer is disabled. To isolate the analog ground plane of the analog-to-digital converter from digital noise sources, optical isolators are used throughout the system on all clock inputs to the analog-to-digital converter.

2.4 The dewar

The NICMOS II Array and its associated optics are housed in an Infrared Laboratories (IRL) HD-8 dewar with two LN_2 vessels. The outer cryogen can cools the radiation shield while the inner can maintains the NICMOS II Array and optics at the 77-K operating temperature. The hold time for the dewar is approximately 20 h.

2.5 The optics

The dewar bolts directly to the prime focus pedestal of the Hale 5-m telescope, looking down at the primary mirror. There are two optical subsystems within the dewar (Figs. 3 and 4). Light first passes through a pair of CaF_2 lenses that serve as a modified Ross corrector[3] to remove residual coma from the image formed by the parabolic 5-m primary mirror. Chromatic aberrations due to this lens pair are minimized because of the lenses' low magnification.

Two filter wheels follow the Ross corrector, each containing eight filter positions. Each wheel has one open position and one blank-off plate for dark current measurements. The 13 remaining positions contain a number of broad- and narrow-band filters for the 1- to 2.5-μm regions: broad-band photometric filters are centered on J band, H band, and K band (1.25, 1.65, and 2.2 μm, respectively); narrow-band filters with 1% to 3% fractional bandwidths are centered on specific spectral lines (e.g., H2, FeII, and Brackett gamma).

After passing through this pair of filter wheels, the light enters an Offner relay, which reimages the image formed by the 5-m primary mirror on a cold stop that rejects background radiation from the telescope. The primary of the Offner relay is Zerodin glass; the secondary of the Offner is a diamond-turned aluminum mirror with a slightly aspheric surface. A hole in the Offner secondary matches the hole in the 5-m primary. Finally, the light is folded once and imaged onto the NICMOS II Array.

The parameters of the optical system were optimized using Code V, and the system performance is quite good. The 128- $\times$ 128-pixel NICMOS II Array has 60-μm pixels that result in 0.7-arcsec pixels and a 90- $\times$ 90-arcsec field of view. Images at the center of the field are usually limited by the seeing at Palomar, which is approximately 1 in. of full-width half-maximum. There is some residual coma at the edges of the field.

2.6 The software

The software used for calibration, test, and the acquisition of science data was developed at JPL by the Infrared Technology Group. The software was developed to run on a PC-based system under a DOS operating environment using the C programming language. A modular design allows the software to be tailored to other systems through the simple modification of the driver program block. Interactive data acquisition and analysis are performed through a user-friendly menu-driven interface. Macro control is also available for the performance of repetitive tasks over long periods of time.

In the data acquisition mode, the user defines the test conditions that specify the file name, the file destination, and the integration time. The user may also specify the number of array resets and reads before each integration cycle. This ensures that all integration nodes are free of residual charge and that the multiplexer begins its integration with known initial conditions. At the Hale Telescope, the PC and controlling software are slaved to the facility's VMS-based computer system. The PC is located in the cage at the base of the telescope, while the dewar, RAPAX electronics, and power supplies are at the telescope's prime focus, communicating over a high-speed coaxial data link.

In the data analysis mode, various math functions are available, including array math, pixel and matrix statistics, and polynomial curve fitting. In the display mode, various pixel mappings are available, including two-dimensional array maps, individual or multiple pixel vs. (x) plots, subregion zoom, individual pixel selection, histograms, and labeling functions including axes labels and titles for both logarithmic and linear plots. Additionally, a near-real-time continuous display mode is available. This mode proved useful in adjusting the focus at the Hale Telescope and in observing long-term drifts in the laboratory.

3. CALIBRATION AND TEST DATA

The primary goal in the radiometric calibration of an infrared camera is to determine the system's transfer function at the operating conditions. This photon-to-digital bit transfer function will depend on numerous internal system parameters and state variables. We will review the significant contributions to this transfer function and comment on its long-term stability.

3.1 Postmultiplexer analog signal chain

The calibration of the RAPAX postreadout electronics requires knowledge of the analog-to-digital converter gain, preamplifier gain, and signal chain bandwidth. Knowledge of the stability of these parameters over time and temperature is also required. To this end, data were acquired independently over a number of days. Figures 5, 6, 7, and 8 are plots of the data taken to establish these parameters. The preamplifier does demonstrate long-term drifts due to temperature variations; these drifts agree with predictions based on published amplifier drift coefficients. The combined results give a conversion of 22.20×10^{-6} V/data number (DN), referred to the input of the RAPAX postreadout electronics.

3.2 Multiplexer source follower gain

As described in section 2.1, there are two source followers operating in series on the NICMOS II Array. These source followers transfer the voltage on the integration node (A of Fig. 1) to the input of the RAPAX electronics. This voltage-to-voltage gain is measured by shorting the anodes (DetSub) and cathodes (VR) of the photodiodes together, stepping this voltage in 0.2-V steps, and taking a frame of data during the array reset for each voltage increment. The resulting slope is calculated on a pixel-by-pixel basis by differencing adjacent frames and dividing by the voltage step. The data are shown in Fig. 9. The gain is quite linear over the range of integration voltages and is equal to 0.64 on average, or approximately 0.80 for each source follower, at 77 K. Note that the source-follower gain is dependent on temperature and operating current through the transconductance of the MOSFETs. Resistivity variations in the silicon substrate may be responsible for the circularly symmetric variations in the data.

3.3 Integration node capacitance

The conversion of photoelectrons created in the photodiode into volts at the integration node is governed by the equation

$$Q = C_{int}(V)\, V$$

where $C_{int}(V)$ is the integration node capacitance described in section 2.1, Q is the total charge, and V is the reset voltage. To determine the capacitance, numerous frames of signal data are collected for increasing integration times. Once the noise is dominated by photon shot noise, the ratio of a signal frame to its corresponding noise frame squared[4] is calculated for a number of integration times and the data are fit by the least-squares method. After scaling for the source-follower gain and other constants according to the formula below, the function $C_{int}(V)$ can be obtained for each pixel.

For the shot-noise limited case,

$$N = \theta_s\, n\, A_d\, t_{int}$$

$$V_s = \frac{N \cdot q}{C_{int}(V)}\, G_{sf}$$

$$\langle V_n \rangle = \frac{\sqrt{N} \cdot q}{C_{int}(V)}\, G_{sf}$$

$$\frac{V_s}{\langle V_n \rangle^2} = \frac{C_{int}(V)}{q\ G_{sf}}$$

where

θ_s	=	photon flux (ph/cm^2/s) at the detector	$C_{int}(V)$	=	integration node capacitance
n	=	quantum efficiency	q	=	coulomb constant
A_d	=	pixel optical area	V_s	=	average output voltage signal
t_{int}	=	integration time	V_N	=	average rms noise derived from the signal variance
G_{sf}	=	effective voltage gain of the readout	N	=	number of photoelectrons

For the sake of this discussion, the average capacitance in the integration region is 0.11 pF per pixel.

3.4 Quantum efficiency

Due to the lack of knowledge of the precise throughput of the foreoptics in the dewar, absolute quantum efficiency measurements were not attempted in the laboratory. Rather, the relative response is mapped in Fig. 10. The 10%, 1-sigma deviation is typical of HgCdTe arrays. Calculation of quantum efficiency using standard stars at the Hale Telescope gives quantum efficiencies of 40% at 1.6 and 2.2 μm with a drop to 25% at 1.2 μm.[5] This decrease in quantum efficiency at the shorter wavelength has not been verified under laboratory conditions.

3.5 Dark current

The dark current due to the reverse bias voltage on these photodiodes is expected to be just a few electrons, given a zero-bias resistance-area product of 1×10^{14} or more. Measurements in the dewar indicate a dark current of 33 e/s under the best dark conditions. This leads to the conclusion that some 300-K photons are getting through the inner shield and to the detector.

3.6 Read noise

The read noise of the device is 46 electrons rms. A map and histogram of the noise are shown in Fig. 11 for a short integration time. The noise of the array remains constant for integration times of less than 20 s, when the dark-current shot noise begins to contribute significantly. Multiple averages of N noise frames for short integrations with N equal to 10, 100, and 1000 samples lead to a square root of N improvement in the variance of the noise. This demonstrates that the correlation time for the noise is longer than 131 s. An average of 10,000 frames failed to improve the variance, suggesting correlated drifts with time scales of less than 20 min.

3.7 Electroluminescence

Data taken on the NICMOS II Array under dark conditions exhibit an increased dark signal in the corner of the array nearest the multiplexer's P-channel, MOSFET output. This effect is shown in Figs. 12 and 13. The magnitude of this signal is independent of the integration time and is thus presumed to be caused by the rapid modulation of the output MOSFET's gate during the readout of the array. The likely mechanism for this effect is electroluminescence in the P-channel, MOSFET output.[6]

3.8 Linearity

An end-to-end linearity analysis was performed[7] on the device, using data collected at the Hale Telescope. A number of integrations were performed with the camera viewing the covered primary 5-m mirror of the telescope. The data were then fit on a pixel-to-pixel basis to a second-order polynomial. The results of this analysis are shown in Fig. 14(a). The histogram and two-dimensional map show the double-peaked distribution of the offset coefficient, A0, and its spatial distribution across the array. The second-coefficient, A1, which is primarily due to quantum efficiency variation in the HgCdTe, is shown in Fig. 14(b). The second-order coefficient (Fig. 14(c)) describes the roll off the array's response. The heavy negative-tending tail of the distribution indicates the nonuniform saturation of the array. The positive coefficients are most probably due to noise in the measurement.

4. OBSERVING AT PALOMAR

The dewar sits at the prime focus of the Hale Telescope and is used in a variety of programs in galactic and extra-galactic astronomy. Figure 15 is an image of the W3 star-forming region taken by Cornell graduate student Tom Mcgeath. Hundreds of individual young stars are apparent in the image. Figure 16 is an image of the infrared luminous galaxy NGC3690. Individual bright spots mark the presence of active star-forming regions that help power the galaxy. Images were taken in the J, H, and K bands, which were combined to give this color picture.

5. ACKNOWLEDGMENT

The research described in this paper was carried out by the Jet Propulsion Laboratory, California Institute of Technology, under a contract with the National Aeronautics and Space Administration.

Reference herein to any specific commercial product, process, or service by trade name, trademark, manufacturer, or otherwise, does not constitute or imply its endorsement by the United States Government or the Jet Propulsion Laboratory, California Institute of Technology.

6. REFERENCES

1. M. Blessinger, K. Vural, W. Kleinhans, M. Rieke, R. Thompson, and R. Rasche, "Low Noise HgCdTe 128 x 128 SWIR FPA For Hubble Space Telescope," N90-21337, *Proceedings of the Third Infrared Technology Workshop*, NASA-TM-102209, National Aeronautics and Space Administration, Washington, pp. 311–320, October 1989.

2. J. L. Schmit and F. L. Stelzer, "Temperature and Alloy Compositional Dependencies of the Energy Gap of Hg_{1-x} Cd_xTe," *J. Appl. Phys.*, Vol. 40, No. 12, pp. 4865–4869, November 1969.

3. F.E. Ross, "LENS systems for the correction of coma in mirrors," *Astrophys* J., Vol. 81, No. 1, pp 156–172, 1935.

4. M. Rieke, E. Montgomery, G.H. Rieke, M. Blessinger, K. Bural, and W. Kleinhans, "Laboratory and Telescope Use of the NICMOS2 128x128 HgCdTe Array," N90-21338, *Proceedings of the Third Infrared Technology Workshop*, NASA-TM-102209, National Aeronautics and Space Administration, Washington, pp. 321–330, October 1989.

5. C. Beichman, "NICMOS Quantum Efficiency," Interoffice Memorandum (internal document), Jet Propulsion Laboratory, Pasadena, October 31, 1991.

6. S. M. Sze, *Physics of Semiconductor Devices, Surface Varactor, Avalanche, Tunneling, and Electroluminescent MIS Diodes*, Chapter 9, pp. 481–487, Wiley-Interscience, 1969,

7. D. Van Buren and T. Jarrett, "PFIRCAM Memo - Linearity Fits to NICMOS Chip," IOM 701-82-021 (internal document), Jet Propulsion Laboratory, Pasadena, February 26, 1992.

Table 1. Summary of the NICMOS II electrical interface

Multiplexer Pin	Signal	Shield	Wire	Ohms
Fsync	R		Constantan	3.1
Mclk	C		Constantan	3.3
Lsync	L		Constantan	3.2
REN	J		Constantan	3.1
Vdd	Y		Copper	0.1
Source Output	e	T	Micro-Coax	6.9
PGate	c	d	Micro-Coax	7.1
Det Sub	a	z	Micro-Coax	6.8
VR	h	F	Micro-Coax	6.8
Vss	H		Copper	0.2

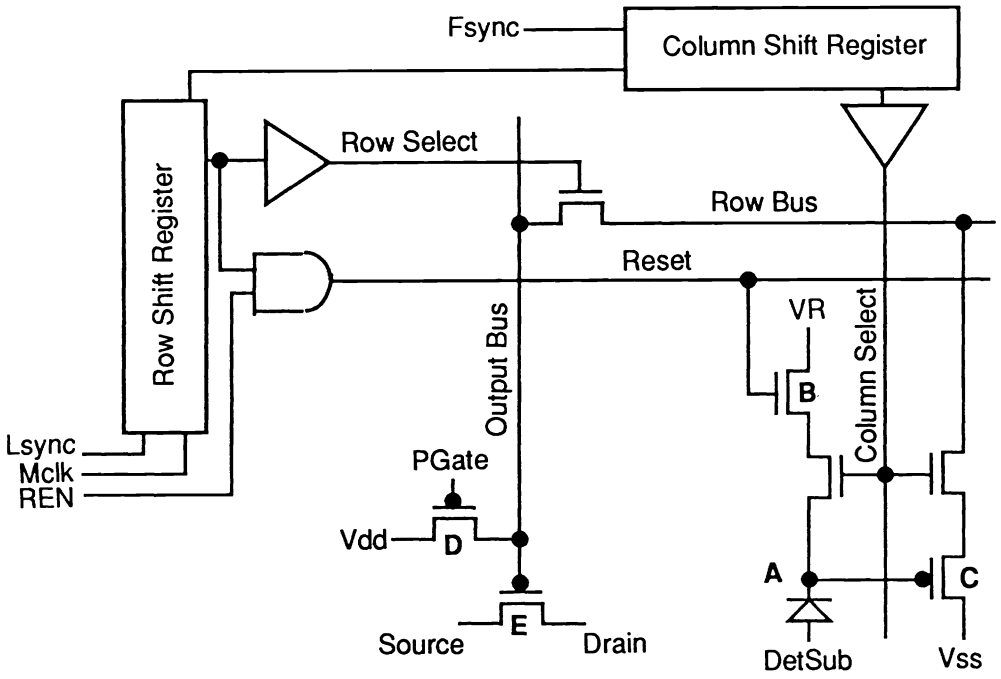

Fig. 1. A circuit schematic for one unit cell of the NICMOS II CMOS multiplexer.

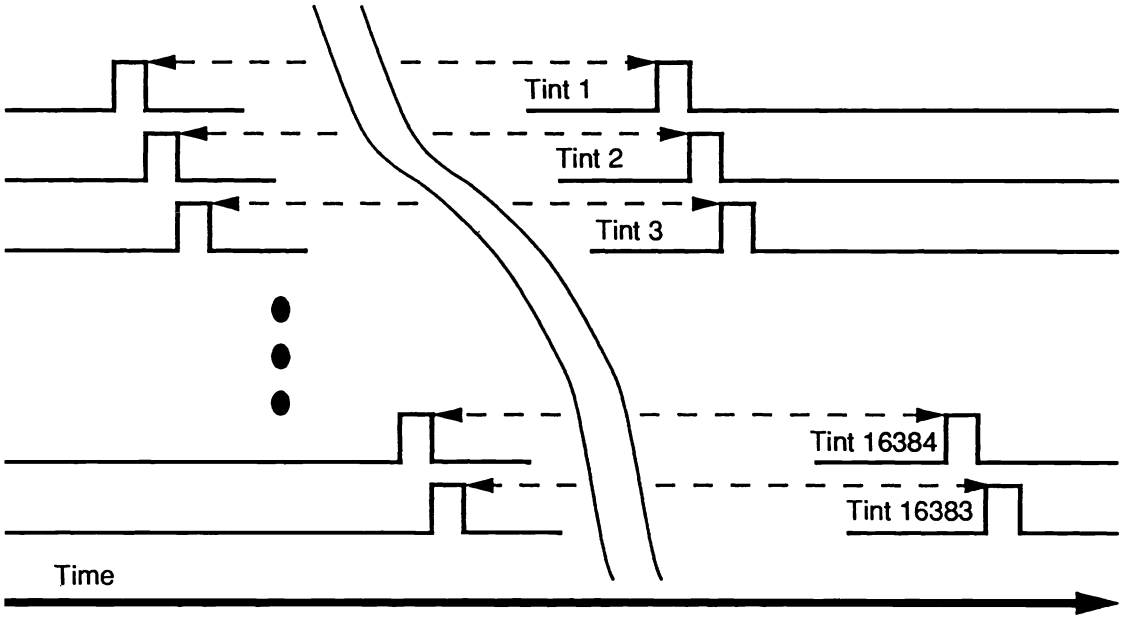

Fig. 2. A conceptual drawing of the nominal timing scheme used for the NICMOS II at JPL.

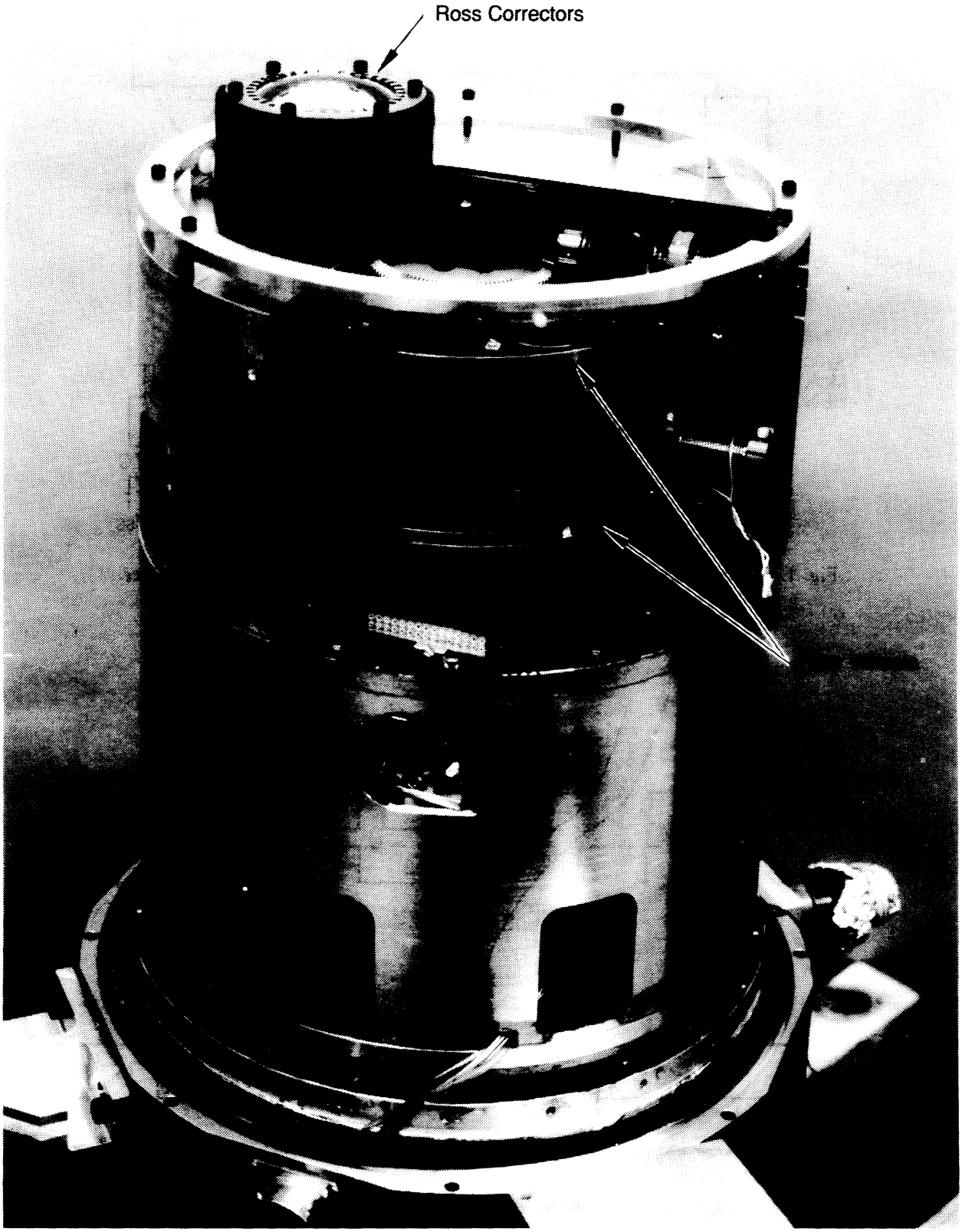

Fig. 3. The IRL HD-8 dewar.

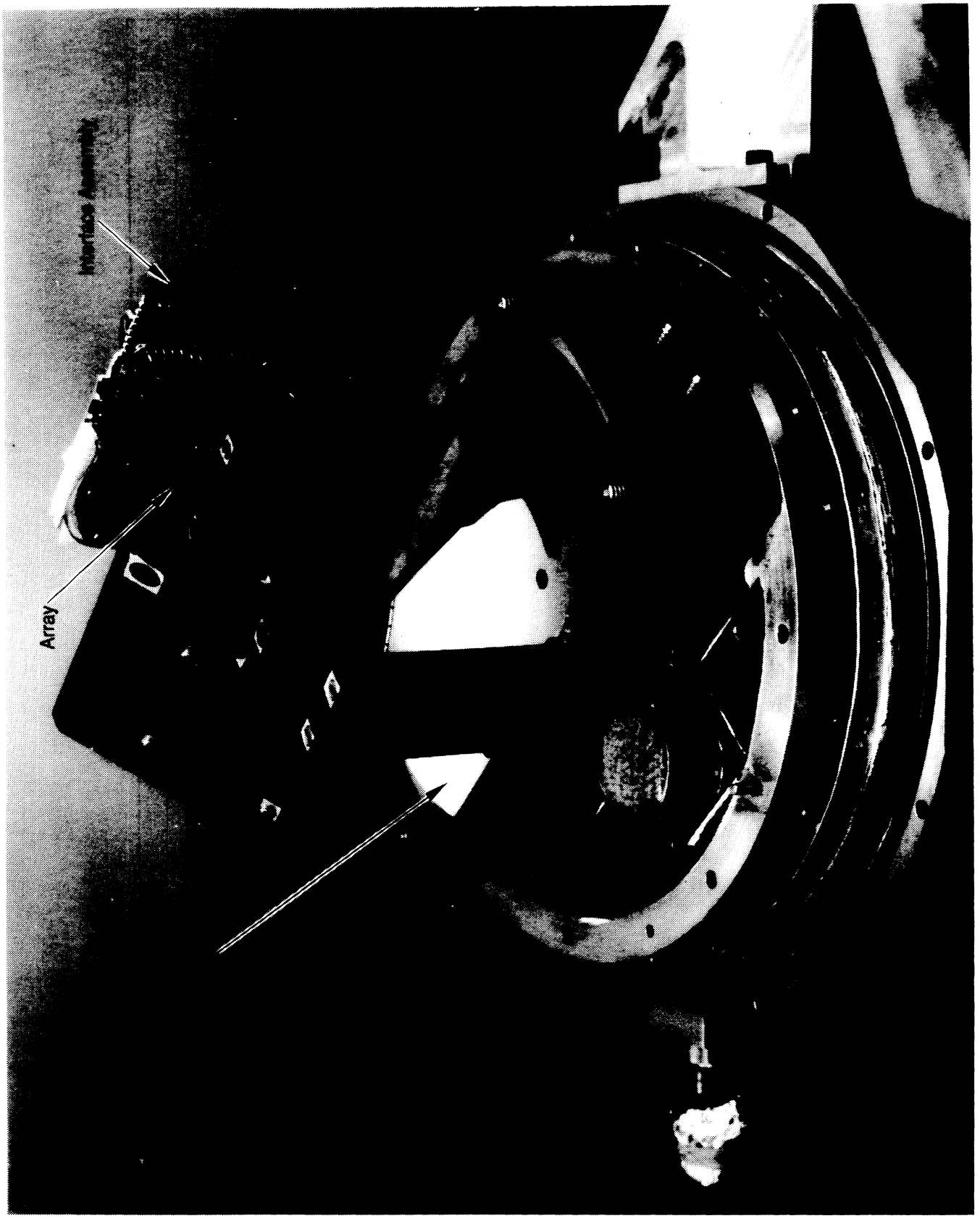

Fig. 4. The dewar with the filter wheel assemblies removed.

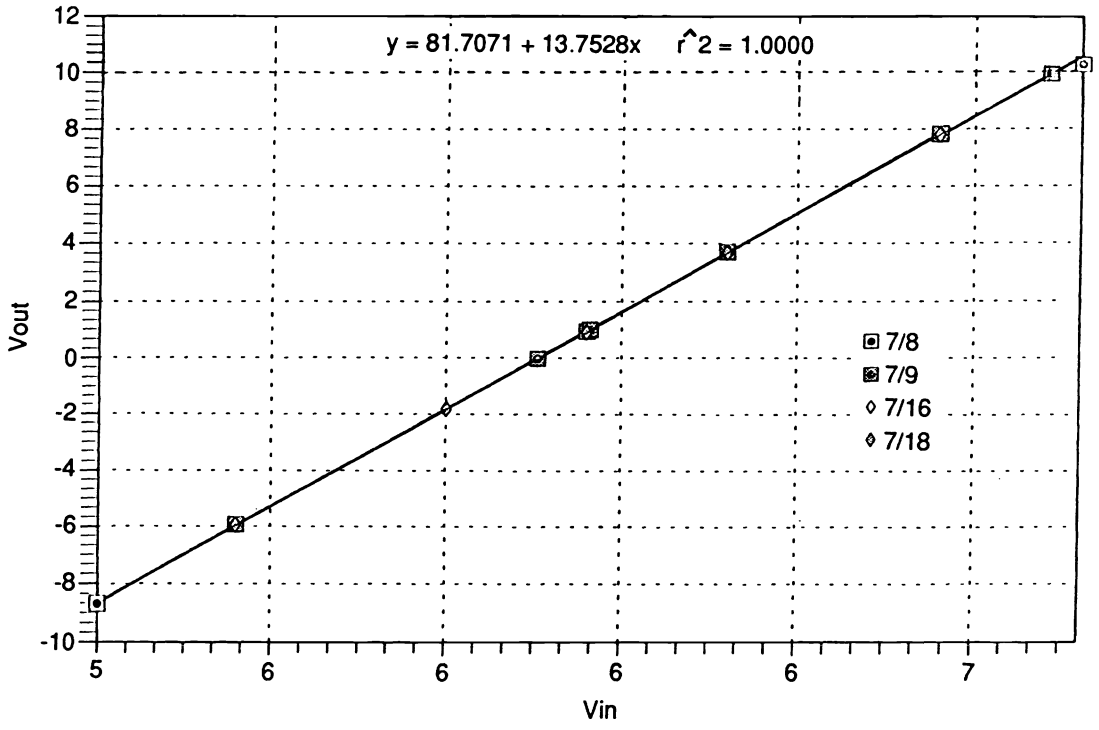

Fig. 5. Gain and offset calibration data acquired for the RAPAX preamplifier. Note that the repeatability is excellent.

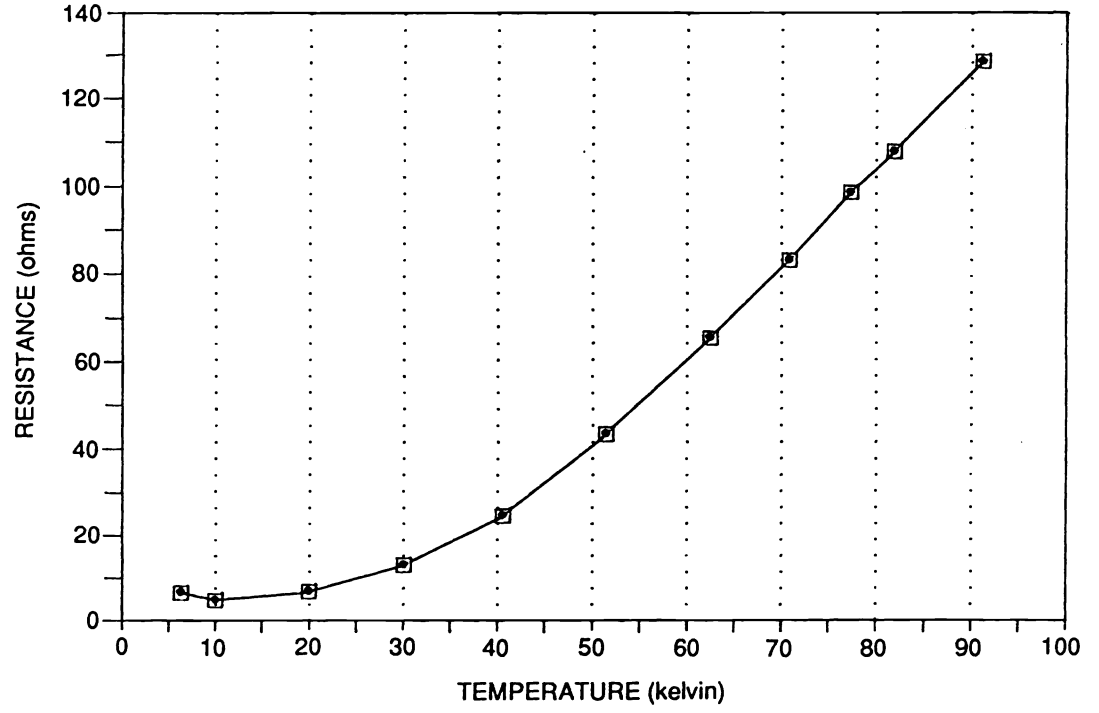

Fig. 6. The temperature calibration curve used to monitor the NICMOS II.

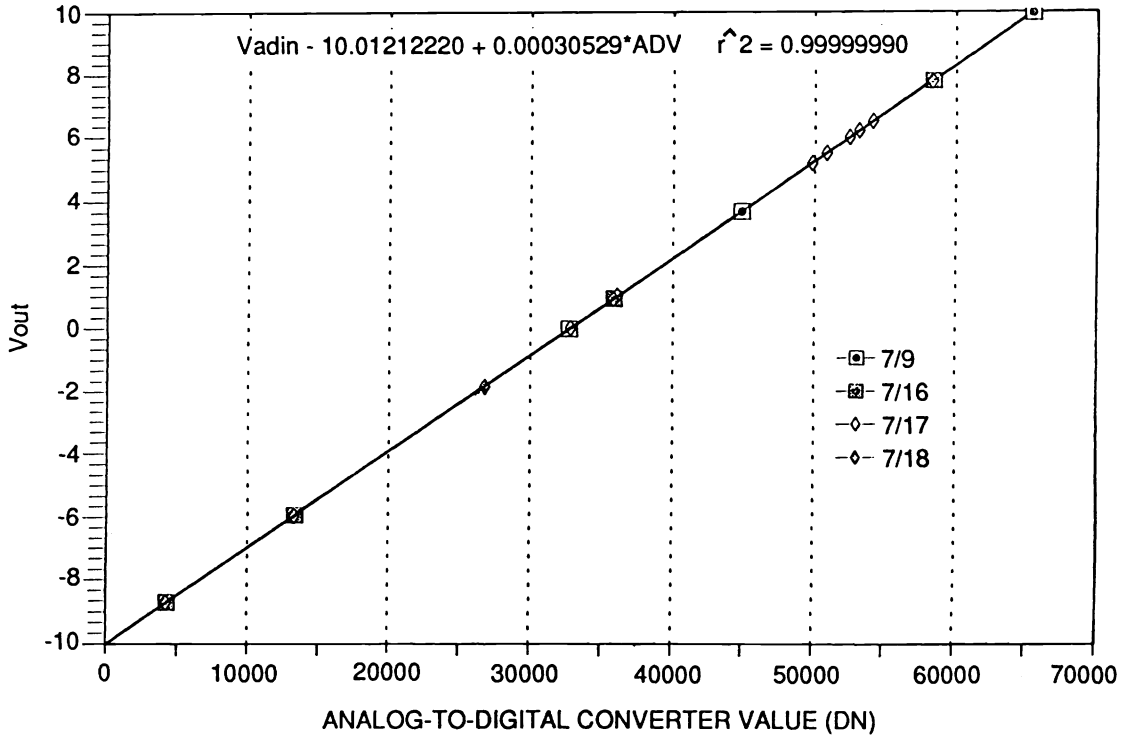

Fig. 7. Gain and offset calibration data for the RAPAX analog-to-digital converter. The data were acquired to demonstrate the stability and repeatability of the converter.

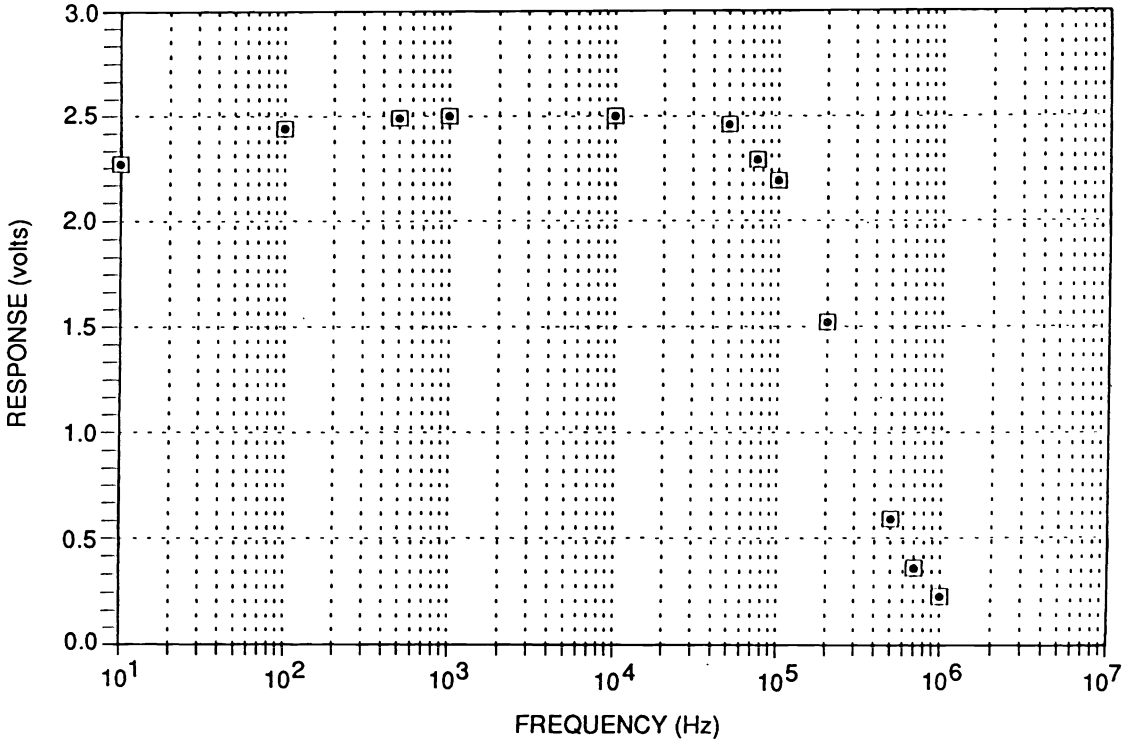

Fig. 8. Frequency response for the RAPAX signal chain with the 3-dB point at 125 KHz.

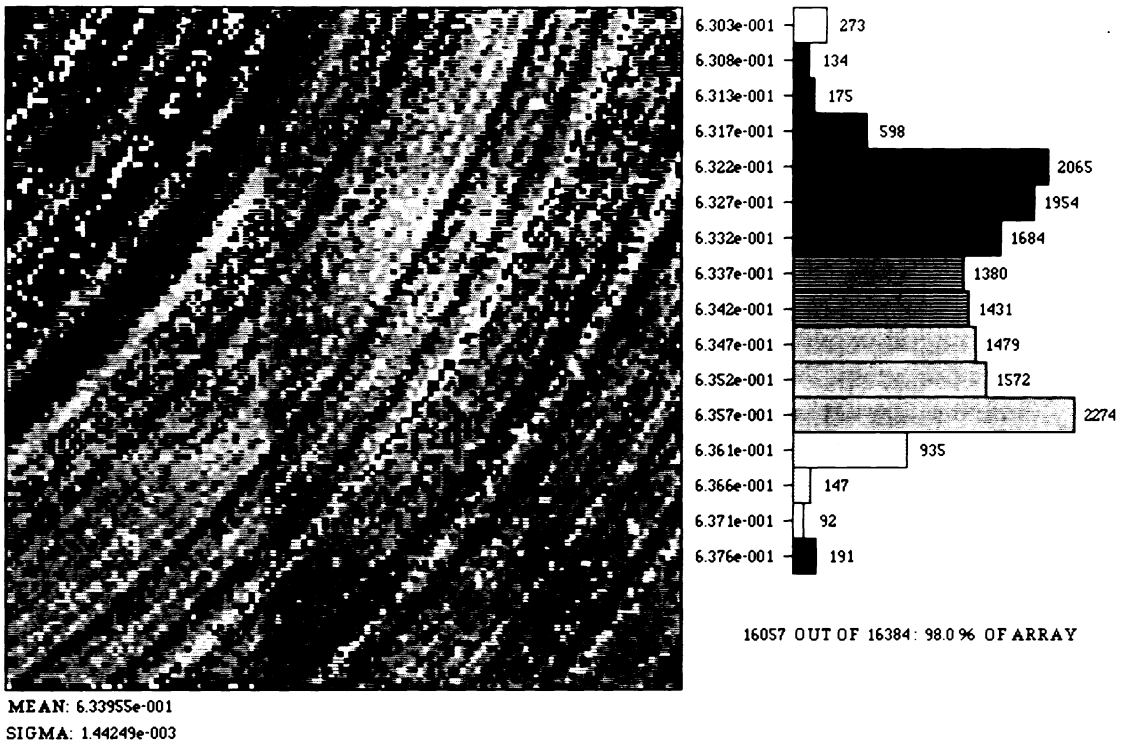

Fig. 9. The combined source-follower gains taken at 77 K.

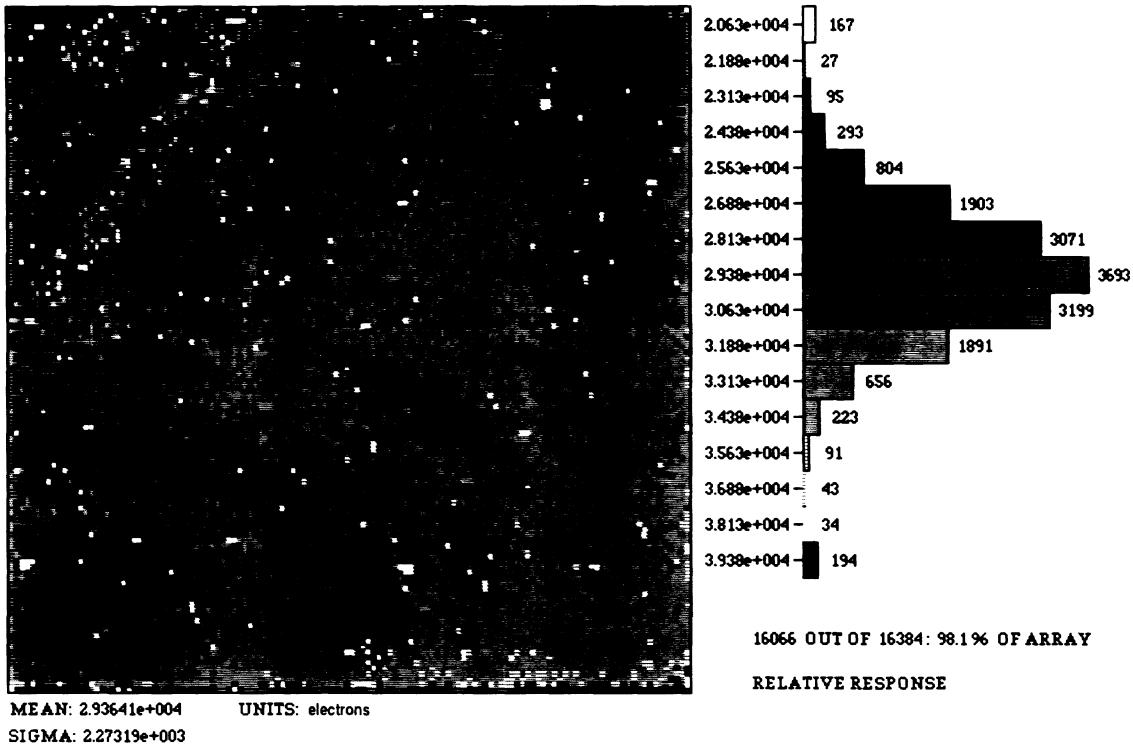

Fig. 10. A relative response frame acquired from 40 contiguous frame averages.

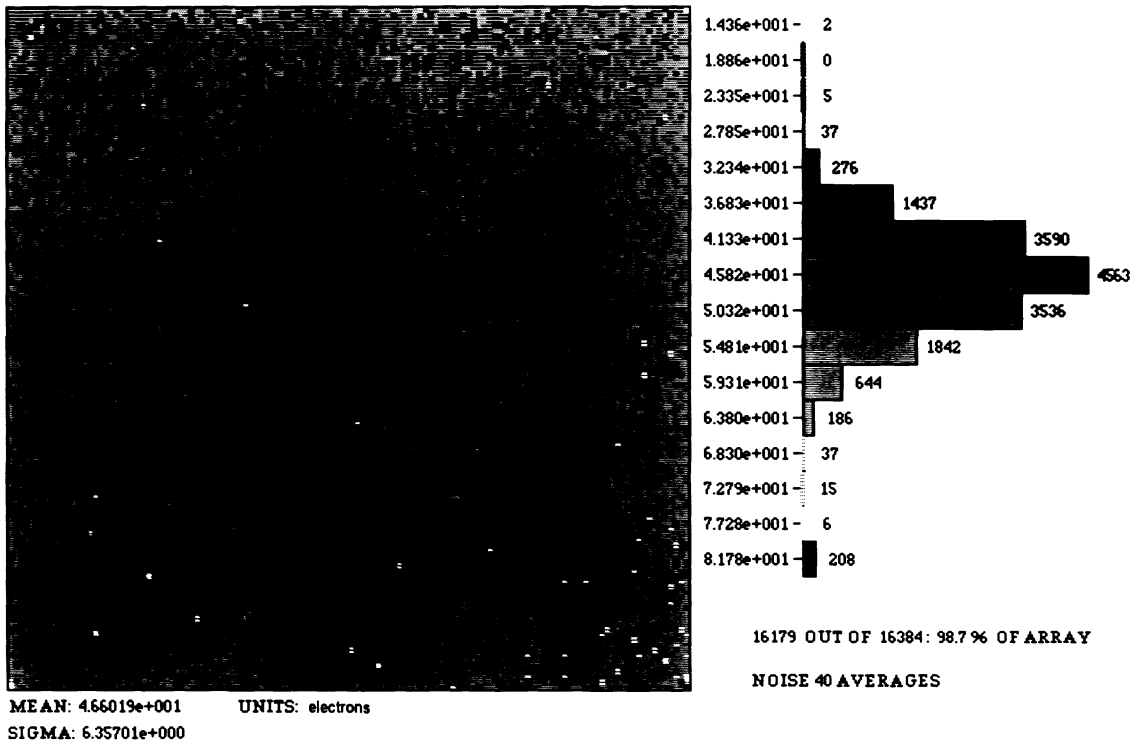

Fig. 11. A noise frame calculated as the variance of 40 signal frames taken under dark conditions.

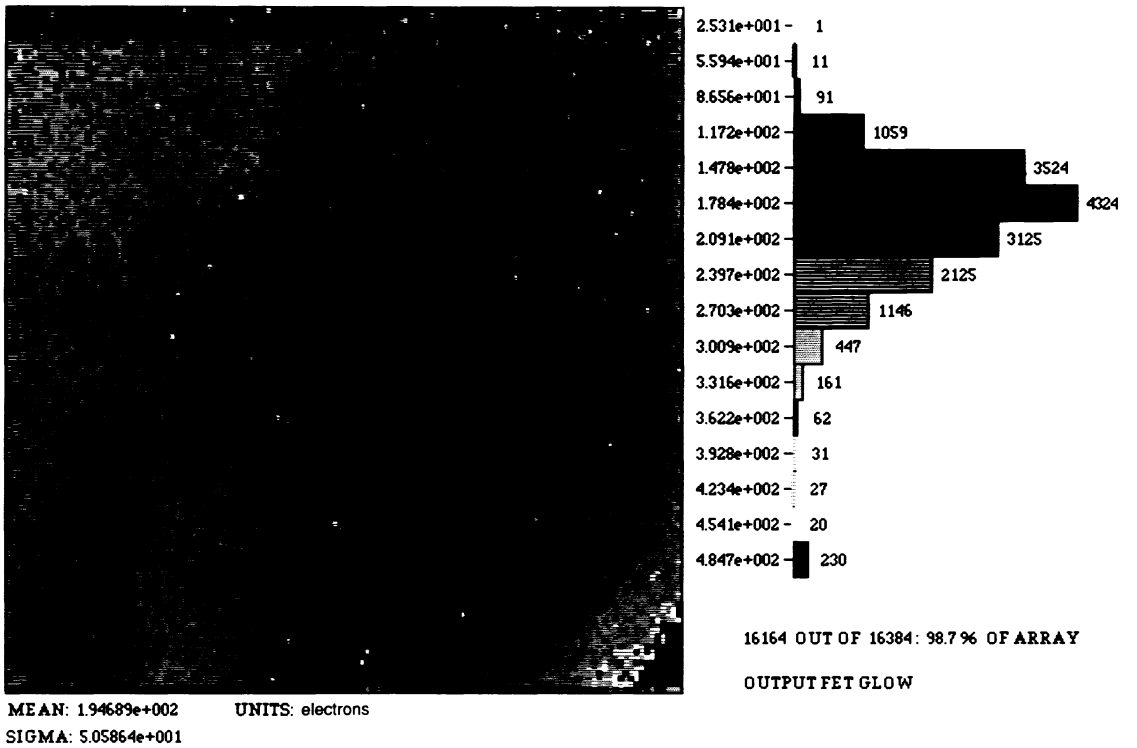

Fig. 12. Evident in this signal frame taken under dark conditions is the electroluminecence of the NICMOS II output PFET.

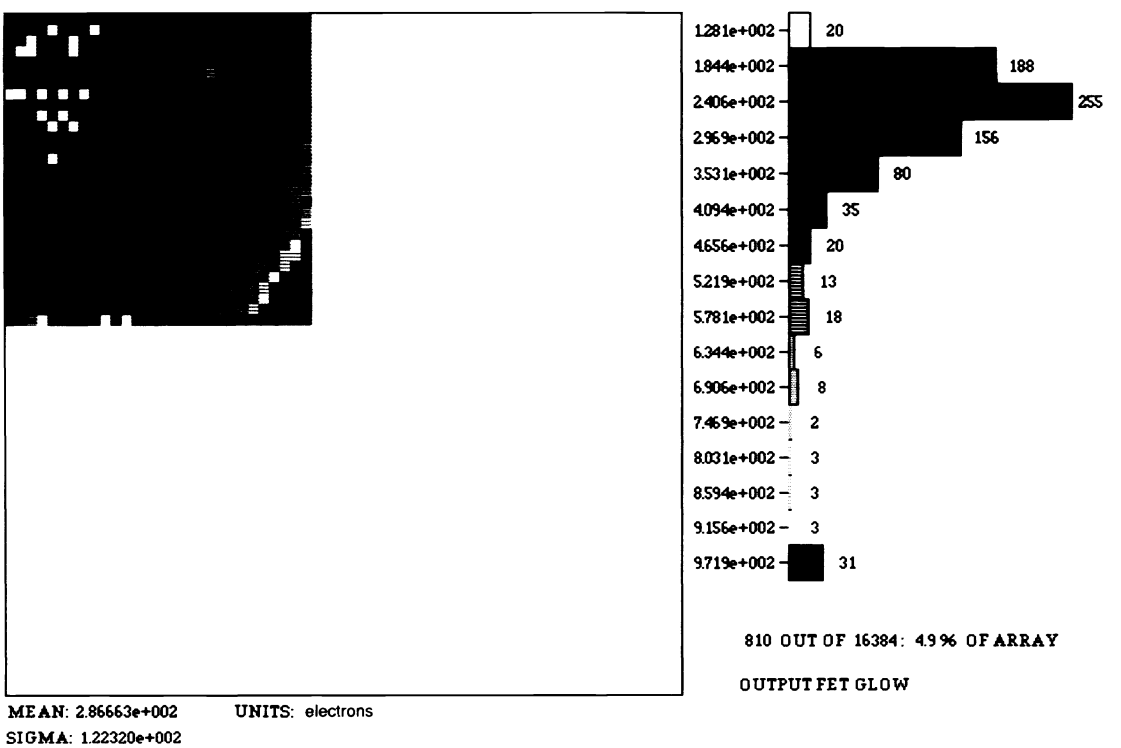

Fig. 13. A subregion zoom of the area affected by the luminescence.

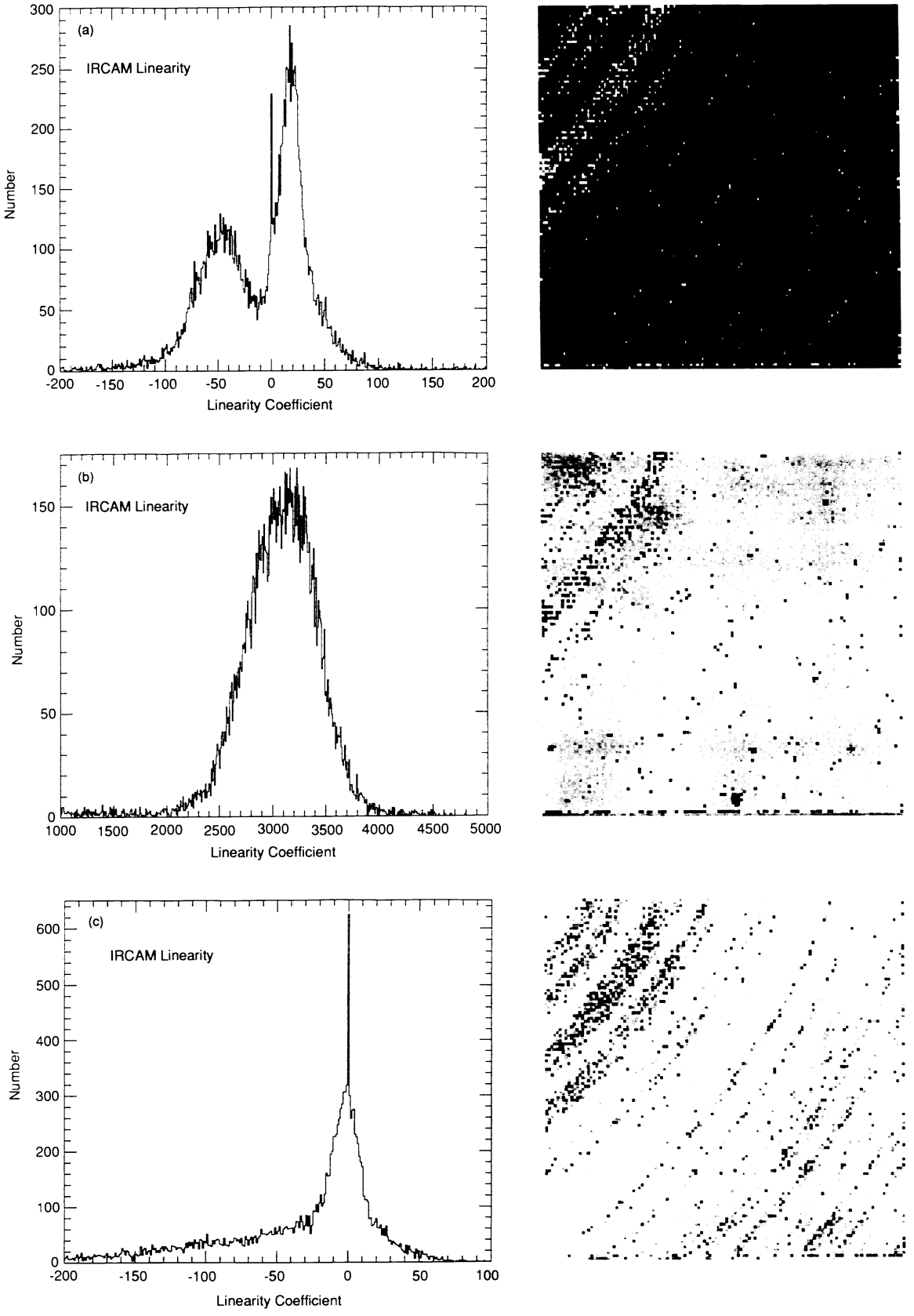

Fig. 14. Histograms and pixel maps for the reduced linearity coefficients (a) A0, (b) A1, and (c) A2.

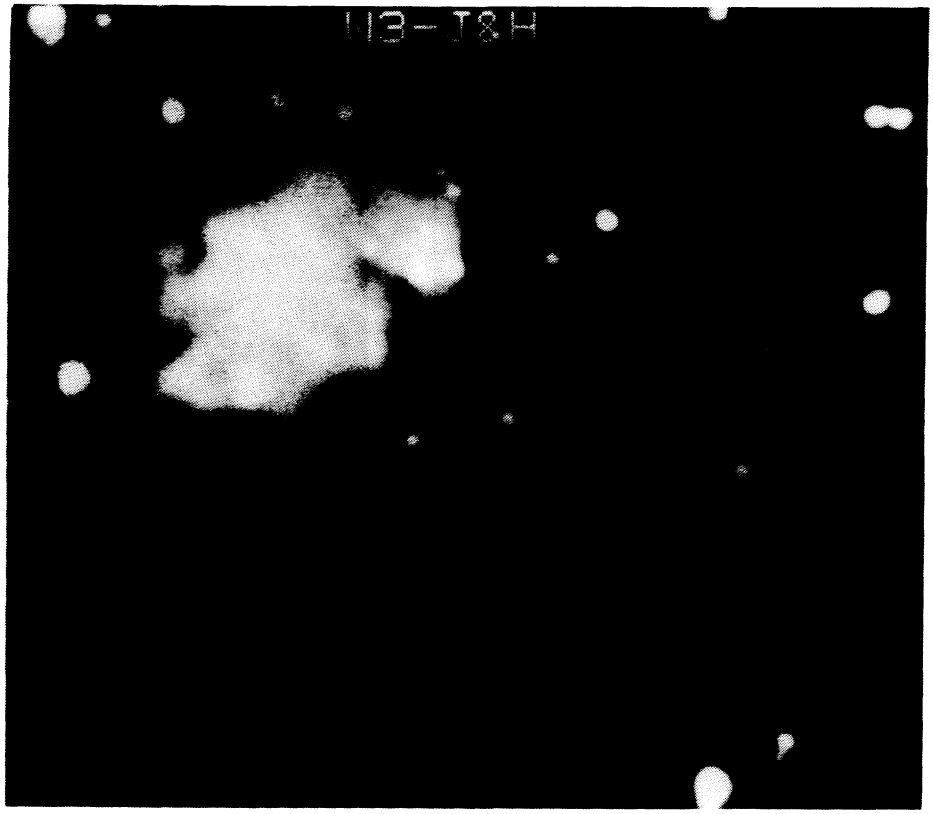

Fig. 15. An H-, J-, and K-band composite image of the W3 star-forming region.

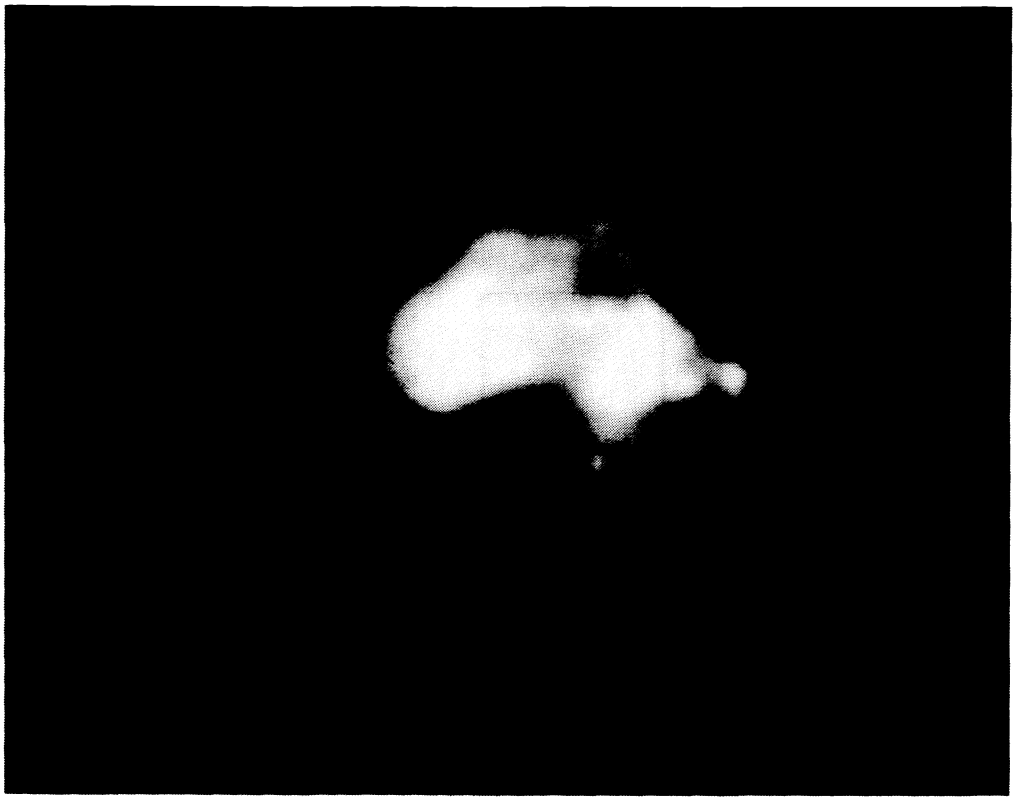

Fig. 16. An H-, J-, and K-band composite image of the infrared luminous galaxy NGC 3690.